Geophys. J. Int. (2002) **151,** 913–923

Contribution at satellite altitude of electromagnetically induced anomalies arising from a three-dimensional heterogeneously conducting Earth, using Sq as an inducing source field

N. Grammatica and P. Tarits

IUEM-UBO, UMR6538 'Domaines Océaniques', Place Nicolas Copernic, 29280 *Plouzané, France.*
E-mails: naphsica@sdt.univ-brest.fr; tarits@sdt.univ-brest.fr

Accepted 2002 July 12. Received 2002 June 10; in original form 2000 December 10

SUMMARY

The induced magnetic signature at satellite altitude associated with crustal and mantle electrical heterogeneities is examined using five different Earth models. The three-dimensional induction problem is solved in these models using the solar quiet daily variation as an inducing source field. Every model has an upper shell representing the land–ocean electrical conductivity distribution. The different models have either a homogeneous mantle or a heterogeneous mantle containing either subduction zones, a ridge system or conductive blocks. Electromagnetic anomalies, presented in the form of geographical maps, are calculated for wavelengths related to spherical harmonics of degrees in the ranges 1–12 and 13–27, respectively. Magnetic anomalies are calculated at an altitude of 400 km and for three different local times: 6, 12 and 18 h.

Key words: electrical conductivity, electromagnetic induction, magnetic anomalies, mantle, numerical modelling, satellite magnetic field.

1 INTRODUCTION

Satellite data are becoming an important part of induction studies. Magnetometers on satellites sample the magnetic field over the entire Earth, thus enabling an estimation of the global response of the Earth to an external field. Furthermore, satellite data enable us to observe short-wavelength magnetic anomalies over the entire surface of the Earth.

The POGO satellites that collected scalar magnetic data from 1965 to 1971 opened the era of global electrical conductivity studies from space. The first global induction study with satellite data was initially performed by Langel (1975) who used the POGO data to estimate ratios of induced to inducing contributions as a function of time. Didwall (1984) studied the POGO data more extensively; she estimated the response functions for several geomagnetic storms and interpreted them in terms of layered conducting Earth models. The MAGSAT satellite was launched in 1979, and for 6 months provided vector data in addition to scalar data. Despite the relatively short satellite lifetime, the data enabled global magnetovariational sounding studies that inferred the electrical conductivity of the mantle (e.g. Didwall 1984; Oraevsky *et al.* 1992a,b, 1993a,b; Olsen 1999). In these studies, a long-period exospheric source field external to the satellite orbit was used; namely a uniform magnetospheric ring current source field parallel to the Earth's dipole axis. In addition, the electrical conductivity of the Earth was assumed to vary only with depth.

Several regional studies (e.g. Oldenburg *et al.* 1984; Egbert & Booker 1992; Schultz *et al.* 1993; Lizarralde *et al.* 1995) have shown that lateral variations of mantle electrical conductivity can be as large as two orders of magnitude. Therefore, these structures might be at the origin of a magnetic signature detectable at satellite altitude apart from the well-known 'coast effect' caused by the ocean–continent electrical conductivity contrasts (e.g. Parkinson 1959, 1980; Menvielle *et al.* 1982). The question of whether the heterogeneous electrical conductivity distribution in the Earth contributes to the magnetic field at satellite altitude has only recently been addressed (e.g. Everett *et al.* 1999; Olsen 1999) and suggests that large-scale heterogeneities can be resolved by magnetic satellite data. These latter studies have used a Dst-type (ring current) source field excitation.

The sources of the magnetic signature over the oceanic areas, especially the Pacific Ocean, are still unknown and are under investigation. Current lithospheric models of long-wavelength anomalies, whether for continental or oceanic crust, require large magnetizations that cannot be accounted for by laboratory measurements on rock samples (e.g. Counil *et al.* 1991; Hayling 1991; Dyment & Arkani-Hamed 1998; Purucker & Dyment 2000). There have been suggestions that the missing magnetization is carried by the upper mantle (e.g. Arkani-Hamed & Strangway 1987; Shive *et al.* 1988; Toft & Arkani-Hamed 1992). However, this hypothesis remains controversial. Clearly, the sources of the oceanic magnetic anomalies need to be investigated further.

Tarits & Grammatika (2000) solved the induction problem in a 3-D electrically conducting Earth with a homogeneous mantle and an uppermost layer with a land–ocean electrical conductivity distribution. They used the solar quiet diurnal field, Sq, as the exospheric

© 2002 RAS

inducing source field and showed that magnetic fields induced by a near-Earth ionospheric source have a magnetic signature up to several nanoteslas at a satellite altitude of 400 km. As expected, they showed that the induced anomaly field is primarily controlled by the coast effect.

In this paper we use the diurnal variation of the magnetic field to investigate the electromagnetic effect of a heterogeneously conducting mantle when a near-Earth ionospheric source field is considered. We show that lateral electrical conductivity contrasts in the upper mantle can contribute magnetic fluctuations at satellite altitude in addition to the coast effect.

The contribution at a satellite altitude of 400 km is estimated for field wavelengths associated with spherical harmonic (SH) degrees in the ranges 1–12 and 13–27. The electromagnetically induced anomalies are calculated at three different local times: dawn, dusk and noon local times.

2 EARTH MODELS

The five models considered in this paper all have spherical layers of different thicknesses surrounding an innermost homogeneous sphere. They encompass an oceanic or a continental-type mantle that is either homogeneous or heterogeneous. The effect of a heterogeneously electrically conducting mantle is investigated using models with large-scale electrically conductive bodies in the upper mantle for which structural information is available. These heterogeneities include subduction zones, the Pacific ridge system and conductive blocks that simulate partial melting zones at various depths inside the mantle. The outermost 4 km thick layer represents the ocean–continent electrical conductivity distribution in which the oceans are taken to have a constant depth of 4 km. The mean conductivity of sea water is taken as 3.3 S m^{-1} and the conductivity of the continents is taken as 0.001 S m^{-1}.

In the first two models (Fig. 1), the uppermost layer overlies a homogeneous 1-D medium representing the mean upper-mantle electrical conductivity structure. The model represented in Fig. 1(a), which will be referred to as CM, is derived from the mantle conductivity profile beneath a continental area (Schultz *et al.* 1993). The model shown in Fig. 1(b), that will be referred to as OM, is derived from the conductivity profile of an oceanic mantle (Lizarralde *et al.* 1995).

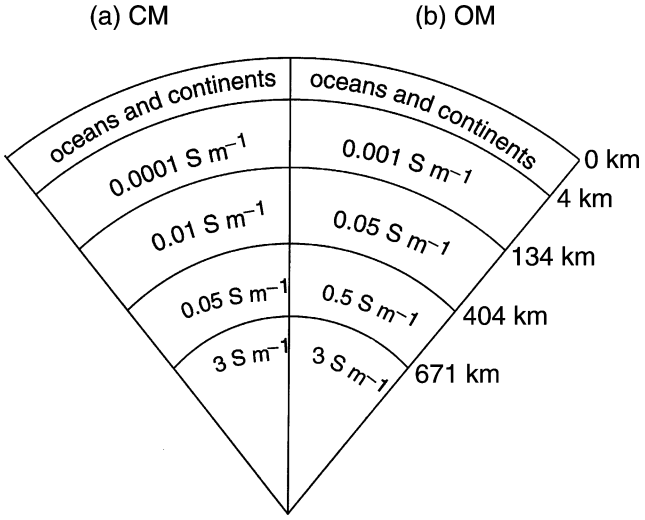

Figure 1. Earth models with a 1-D electrical conductivity distribution in the mantle: (a) continental-type electrical conductivity structure (CM); (b) oceanic-type electrical conductivity structure (OM). The radial axis is not drawn to scale.

The third model has subducting slabs in the mantle (Fig. 2) and is referred to as OMSL. Structural information for subduction zones at the scale of the upper mantle is available from a combination of seismological and geoid data (e.g. Hagger & Clayton 1989). The dipping slabs are considered to be vertical down to approximately 400 km and have an electrical conductivity of 2×10^{-3} S m^{-1}. This electrical conductivity value is used to examine the electromagnetic effect of slabs that are electrically resistive with respect to the surrounding medium. The resistive slab corresponds to a dehydrated oceanic lithosphere devoid of sediments (e.g. Wannamaker *et al.* 1989).

The fourth model has an oceanic mantle (Fig. 3) containing conductive blocks and is referred to as OM2B. Various studies have identified the presence of conductive zones in the mantle under the Pacific Ocean floor (e.g. Larsen 1975; Oldenburg *et al.* 1984; Lizarralde *et al.* 1995). In model OM2B, these zones are represented as conductive blocks (Fig. 3a) with a thickness of 50 km and an electrical conductivity of 1 S m^{-1}. The blocks are centred at depths of 180 km in the North Central Pacific and 130 km below the Juan de Fuca ridge (Fig. 3b) and correspond to the deep-seated conduction zones observed from ocean bottom magnetotelluric soundings (e.g. Filloux 1980; Oldenburg *et al.* 1984; Tarits 1986). Their respective lateral dimensions are 30 and 15 km and their locations are shown on Fig. 3(b).

The final or fifth model uses a schematic representation of the North and South Pacific ridge system from the East Pacific Rise to the Juan de Fuca ridge (Fig. 4). This model is referred to as OMR. The cooling lithosphere on either side of the ridge is represented by a series of conductive layers with a total thickness of 130 km as part of an oceanic mantle conductivity structure (e.g. Tarits & Jouanne 1990). The ridge model is based on the cooling of the oceanic lithosphere as it ages (e.g. Sclater *et al.* 1980). The extent of the conductive structure widens as the depth increases, with an electrical conductivity that decreases as we go further away from the ridge axis (e.g. Oldenburg *et al.* 1984). The maximum horizontal extent of the conductive structure of the ridge model reaches approximately 3000 km at 130 km depth (Fig. 4). This simple representation of a ridge is sufficient to show that an extended structure can contribute an electromagnetically induced signal at satellite altitude.

3 THE NUMERICAL SOLUTION OF THE INDUCTION PROBLEM

3.1 Solving the induction problem

The mantle is divided into spherical shells. The electrical conductivity within each shell may be uniform or it may vary horizontally, but it may not vary radially. The stack of shells starts from a homogeneous inner sphere of finite conductivity and ends at an upper boundary above which the medium is insulating. Under the quasi-static approximation and in the frequency domain (assuming a time dependence of $e^{i\omega t}$), the governing equations in the inner sphere are

$$\begin{aligned} \nabla \cdot \mathbf{B}(\mathbf{r}, \omega) &= 0 \\ \nabla \times \mathbf{E}(\mathbf{r}, \omega) &= -i\omega \mathbf{B}(\mathbf{r}, \omega) \\ \nabla \times \mathbf{B}(\mathbf{r}, \omega) &= \mu \sigma_c \mathbf{E}(\mathbf{r}, \omega) \end{aligned} \tag{1}$$

and the governing equations in the mantle are

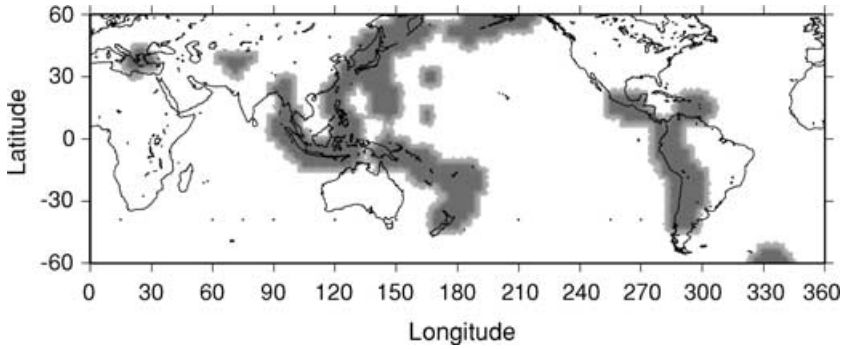

Figure 2. Distribution of subducting slabs. This distribution is used in model OMSL.

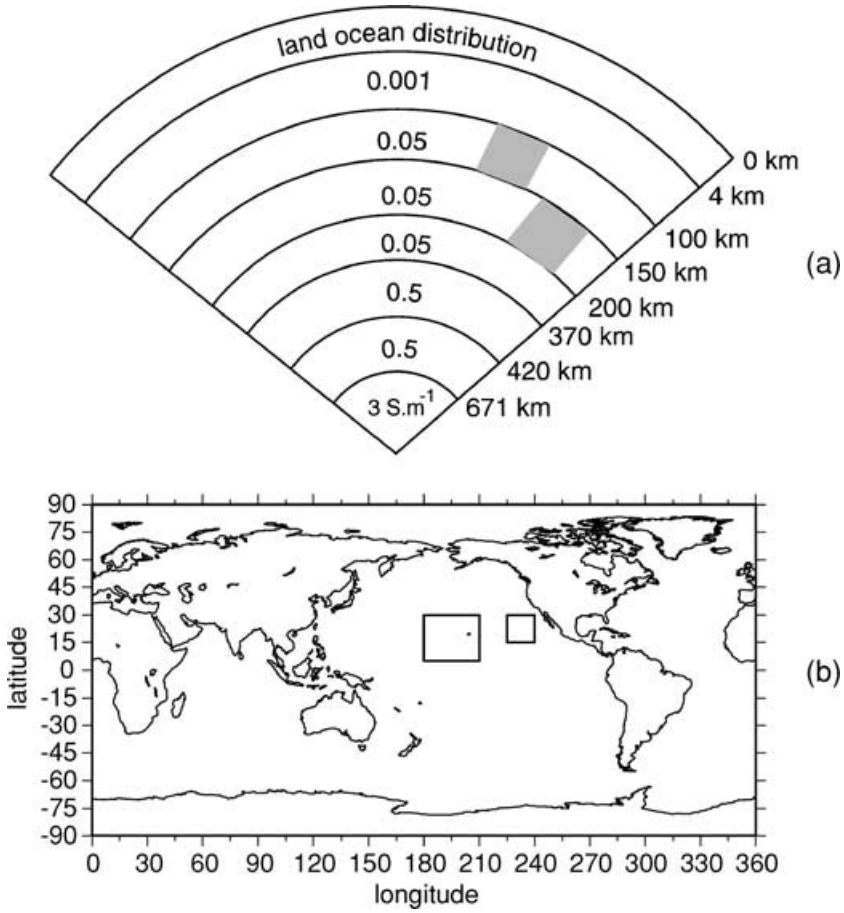

Figure 3. (a) Earth model including a land–ocean distribution and conductive blocks under the Pacific Ocean floor. This is model OM2B where the two blocks have an electrical conductivity of 1 S m^{-1}. The radial axis is not drawn to scale and values in each layer represent electrical conductivities in units of S m^{-1}. (b) Locations and sizes of the two conductive blocks under the Pacific Ocean floor.

$$\nabla \cdot \mathbf{B}(\mathbf{r}, \omega) = 0$$
$$\nabla \times \mathbf{E}(\mathbf{r}, \omega) = -i\omega \mathbf{B}(\mathbf{r}, \omega) \tag{2}$$
$$\nabla \times \mathbf{B}(\mathbf{r}, \omega) = \mu \sigma_{\mathrm{m}}(\mathbf{r}) \mathbf{E}(\mathbf{r}, \omega)$$

where μ is the magnetic permeability in vacuum, and **B** and **E** are the magnetic and electric fields. The value σ_{c} is the conductivity of the inner sphere. The mantle conductivity $\sigma_{\mathrm{m}}(\mathbf{r})$ depends on the position vector **r**. The source of the **E** and **B** fields is outside the Earth in the ionosphere or in the magnetosphere. Above the Earth's surface, the atmosphere is insulating, eq. (2) is still valid but with $\sigma_{\mathrm{m}}(\mathbf{r}) = 0$.

The solution to eq. (2) is written as (the dependence to ω is implicit):

$$\mathbf{E}(\mathbf{r}) = \mathbf{E}_n(\mathbf{r}) + \mathbf{E}_a(\mathbf{r})$$
$$\mathbf{B}(\mathbf{r}) = \mathbf{B}_n(\mathbf{r}) + \mathbf{B}_a(\mathbf{r}), \tag{3}$$

where the normal fields, $(\mathbf{E}_n, \mathbf{B}_n)$, are the solution for a homogeneous inner sphere ($\sigma = \sigma_{\mathrm{c}}$) and an insulating mantle ($\sigma_{\mathrm{m}} = 0$) subject to a source field external to the Earth. The anomalous fields, $(\mathbf{E}_a, \mathbf{B}_a)$ represent the effects of mantle conductivity. The equations that govern the normal fields $\mathbf{E}_n(r)$, $\mathbf{B}_n(r)$ are:

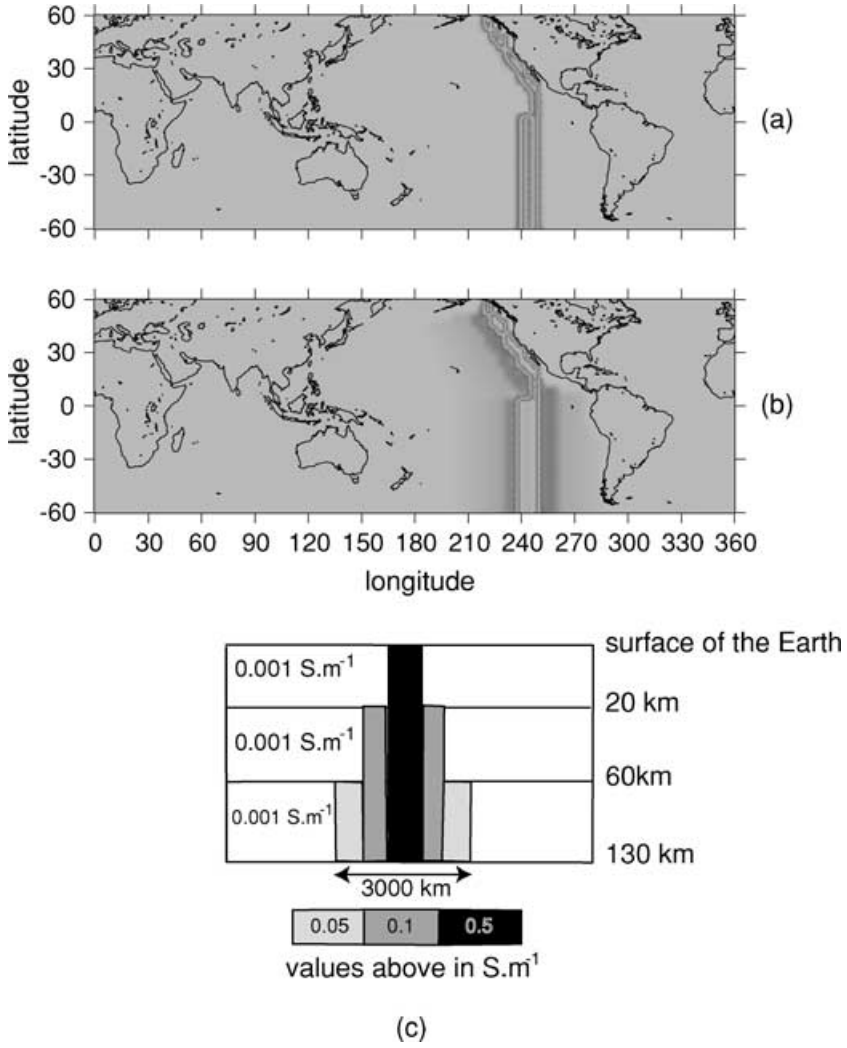

Figure 4. Model of the East Pacific Rise (model OMR) and the Juan de Fuca ridge showing the lateral extent of the ridge between (a) 20 and 60 km, (b) between 60 and 130 km, and (c) a schematic representation of the electrical conductivity distribution of the ridge model.

$$\left.\begin{aligned}\nabla \times \mathbf{E}_n(\mathbf{r}) &= -i\omega \mathbf{B}_n(\mathbf{r}) \\ \nabla \times \mathbf{B}_n(\mathbf{r}) &= \mu\sigma_c \mathbf{E}_n(\mathbf{r})\end{aligned}\right\} \text{in the inner sphere} \tag{4}$$

$$\left.\begin{aligned}\nabla \times \mathbf{E}_n(\mathbf{r}) &= -i\omega \mathbf{B}_n(\mathbf{r}) \\ \nabla \times \mathbf{B}_n(\mathbf{r}) &= 0\end{aligned}\right\} \text{in the mantle.} \tag{5}$$

Subtracting eq. (4) from eq. (1) and eq. (5) from eq. (2), we obtain the set of equations for the anomalous fields:

$$\left.\begin{aligned}\nabla \times \mathbf{E}_a(\mathbf{r}) &= -i\omega \mathbf{B}_a(\mathbf{r}) \\ \nabla \times \mathbf{B}_a(\mathbf{r}) &= \mu\sigma_c \mathbf{E}_a(\mathbf{r})\end{aligned}\right\} \text{in the inner sphere} \tag{6}$$

$$\left.\begin{aligned}\nabla \times \mathbf{E}_a(\mathbf{r}) &= -i\omega \mathbf{B}_a(\mathbf{r}) \\ \nabla \times \mathbf{B}_a(\mathbf{r}) - \mu\sigma_m(\mathbf{r})\mathbf{E}_a(\mathbf{r}) &= \mu\sigma_m(\mathbf{r})\mathbf{E}_n(\mathbf{r})\end{aligned}\right\} \text{in the mantle.} \tag{7}$$

This separation of the field into normal and anomalous components allows us to solve the problem in two steps (Lognonné, 1989). First, eqs (4) and (5) are solved to obtain the normal field caused by the known source field. This normal field is then used as the source term for generating the anomalous field, using the $\mathbf{E}_n$ term in eq. (7).

The fact that the boundaries in our Earth's model are all spherical surfaces, means that our equations can be solved most easily in spherical coordinates, (r, θ, φ), where θ and φ are the colatitude and eastward longitude, respectively. Although the laterally varying conductivity removes spherical symmetry, it is useful to employ spherical harmonic expansions when solving the equations. Accordingly, the electric and magnetic fields are expanded into a generalized spherical harmonics (GSH) series that is a natural basis for vector fields (see Appendix, e.g. Phinney & Burridge 1973).

The GSH expansions of the **E** and **B** fields in eqs (4)–(7) are used to obtain differential equations for the GSH coefficients in these expansions. The resulting equations are first-order ordinary differential equations in the radial coordinate r. The normal field can be completely determined in the mantle by specifying the values of the SH components of the radial magnetic and electric fields at the Earth's surface for a given source field. The equations for the anomalous field are obtained from the GSH expansion of eqs (6) and (7).

3.2 Source field and numerical applications

In a previous paper (Tarits & Grammatika 2000), the diurnal variation Sq and its first two harmonics were inferred by examining temporal variations of the magnetic field measured at 67 observatories during the MAGSAT mission. We showed that

magnetic fields induced by this source field have, at a satellite altitude of 400 km, a magnetic signature of up to several nanoteslas associated with the ocean–continent distribution. In this paper the same source field as in Tarits & Grammatika (2000) is used in the numerical solution of the induction problem.

The electromagnetic induction algorithm is run for the Sq periods (T) of 8, 12 and 24 h, in the spatial domain using a regular grid of 96×48 meshes and in the spectral domain using a spherical harmonic expansion (SHE) to degree (l) and order (m) 27. The SHE degrees and orders for the source field are $l = 2; m = 1$ ($T = 24$ h), $l = 3; m = 2$ ($T = 12$ h) and $l = 4; m = 3$ ($T = 8$ h). In a 1-D Earth model, the induced internal field has exactly the same SHE as the source field. In a 3-D Earth model, the induced internal field has energy in all degrees and orders as a result of the coupling between the source field and the lateral variations of electrical conductivity in the crust and mantle.

The induced magnetic response of the different models to induction at the three periods (8, 12 and 24 h) is calculated at the surface of the Earth. The magnetic field is subsequently continued upwards to 400 km following the hypothesis of Langel *et al.* (1996) that the ionosphere can be modelled by sheet currents flowing in a thin conducting shell at an altitude of 110 km. The magnetic field is calculated at dawn ($t_{\text{local}} = 6$ h), dusk ($t_{\text{local}} = 18$ h) and noon ($t_{\text{local}} = 12$ h) local times and is expressed in the spatial and time (UT) domains by using a combination of geographical coordinates and UT times such that the time value of the calculated field is associated with the same local time all over the Earth. The results are presented in the form of magnetic maps.

4 RESULTS

4.1 Introduction

The inclusion of electrical conductivity heterogeneities in the mantle generates a redistribution of the induced electrical currents and consequently a change in the electromagnetic field that would be associated with currents in a homogeneous medium.

The mantle electrical conductivity heterogeneities and the surface electrical conductivity contrasts produce magnetic effects that can be split into three terms; a term accounting for the magnetic effect of the surficial structures without mantle structures, a term accounting for the effect of mantle structures without the surficial effect and a coupling term accounting for the mutual effect between surficial and deep structures.

In this study the induced internal magnetic field is examined for two wavelength ranges corresponding to SH degrees in the ranges 1–12 and 13–27. The wavelengths associated with the range 1–12 correspond to a superposition of internal induced and external inducing fields. Only the induced part is considered in this paper. The range 1–12 is selected to show the contribution of induced fields that contain the longest wavelengths. The range 13–27 is selected to investigate the contribution of induced fields in the same wavelength range as the crustal field. The knowledge of the contribution of electromagnetically induced fields in the same wavelength range as crustal fields constitutes important information when deriving static lithospheric magnetic anomaly maps (Hermance 1982).

4.2 Induced magnetic field related to the conductivity heterogeneities in the mantle

Fig. 5 represents the energy spectra of the internal fields induced in models OM, OMSL, OM2B and OMR at $T = 24$ h. The degrees of the SH coefficients describing the induced field are contained in the range 1–27. Spectra at 12 and 8 h exhibit similar characteristics and are not shown.

Fig. 5(a) represents the energy spectrum for all degrees from 1 to 27 and Fig. 5(b) represents the energy spectrum for degrees above those of the source field ($l > 4$). It can be seen that the induced internal field predominates for degrees up to four. This results from induction at the source scale in the mean Earth plus the effect of the

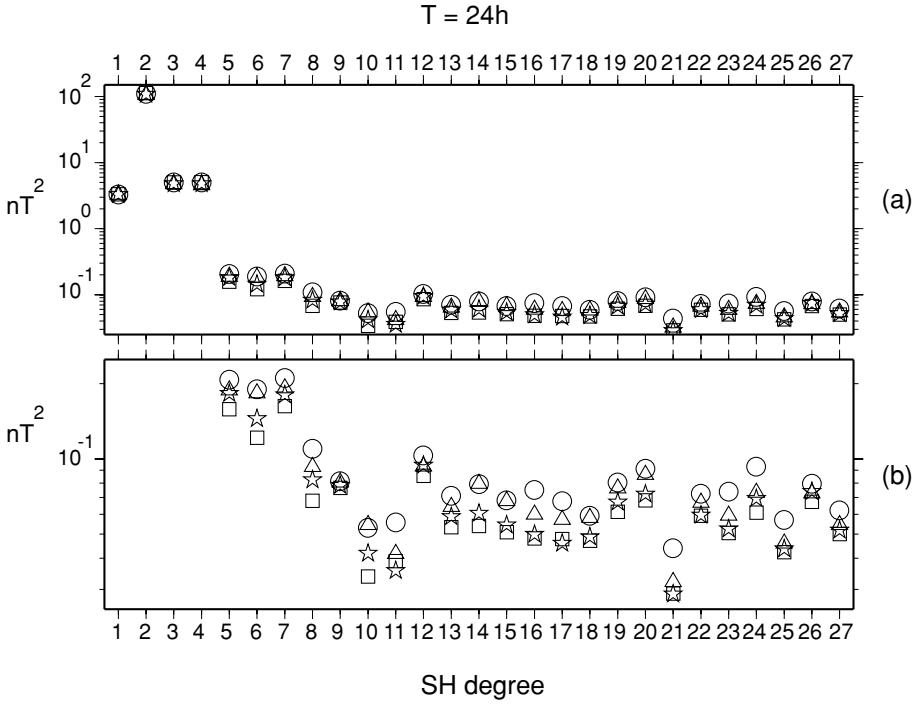

Figure 5. Energy spectrum of the internal magnetic fields induced in models OM (star), OMSL (triangle), OM2B (square) and OMR (circle) for SH degrees in the range (a) 1–27 and (b) 5–27.

lateral variations of conductivity. At all other degrees and orders, the induced internal magnetic field results exclusively from the lateral variations of electrical conductivity.

In order to retrieve the induced magnetic field due exclusively to the electrical heterogeneity in the mantle, the induced magnetic field related to the coast effect is subtracted from the induced magnetic field calculated for the different models OMSL, OM2B and OMR. As mentioned at the beginning of this paper, the coast effect refers to the electromagnetically induced anomaly field that arises from the electrical conductivity contrast of the oceans and continents in a surficial layer. The residual field that is obtained after subtraction contains the induced magnetic anomaly field associated with the mantle heterogeneity plus the mutual coupling between this heterogeneity and the coast effect. Tarits & Menvielle (1983) show that for short wavelengths of the induced magnetic field (i.e. wavelengths shorter than the inducing field wavelength) and for a penetration depth exceeding the thickness of the heterogeneously electrically conducting earth layer, the mutual coupling term is negligible.

The average electrical conductivity of the mantle in our models and the periods of the Sq-inducing source field result in a penetration depth that is within the conditions that Tarits & Menvielle (1983) specified. It will be shown that the mutual coupling is indeed more important for SH degrees in the 'long-wavelength' range 1–12 than for SH degrees in the 'short-wavelength' range 13–27.

4.2.1 Residual magnetic anomaly field for SH degrees in the range 1–12

Figs 6(a) and (d) show the vertical component Z ($Z = -B_0$, see Appendix) of the induced internal magnetic anomaly field calculated for models OMSL and CMSL for SH degrees in the range 1–12, at noon local time. Figs 6(b) and (c) represent the residual magnetic

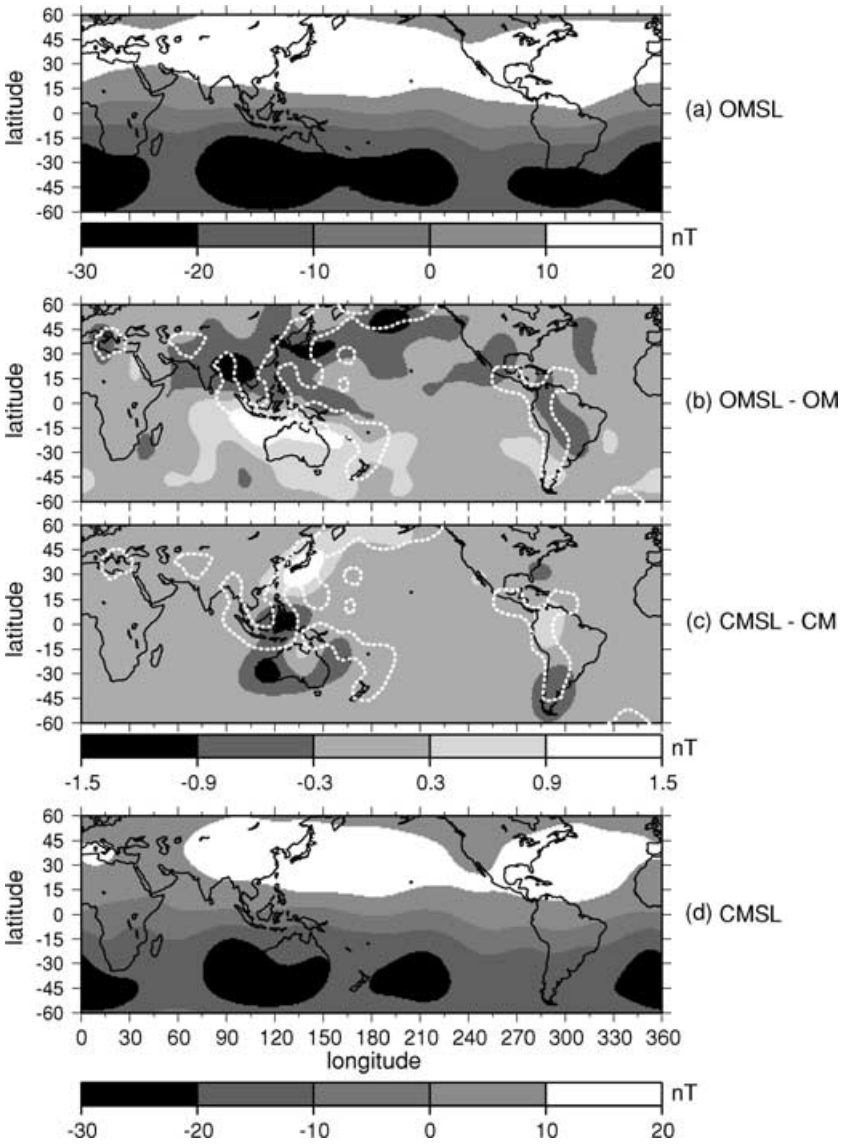

Figure 6. (a) and (d) Z component of the electromagnetically induced field for OMSL and CMSL, respectively. (b) and (c) Z component of the residual field for (OMSL–OM) and (CMSL–CM), respectively. Local time = noon. The SHE of the calculated fields contain SH degrees in the range 1–12. The slabs in OMSL have an electrical conductivity of 0.002 S m^{-1}. The second grey-scale from the bottom describes (b) and (c). The dotted white lines in (b) and (c) are a schematic representation of the subducting slabs.

Table 1. Minimum (<0) and maximum (>0) amplitudes (in nanoteslas) of the residual field at satellite altitude for SH degrees in the range 1–12, calculated for (OMSL–OM) and (CMSL–CM) at dawn, dusk and noon local times. The slabs in OMSL have an electrical conductivity of 0.002 S m^{-1}.

Model	Dawn min/max (nT)	Dusk min/max (nT)	Noon min/max (nT)
OMSL–OM	−1.0/1.0	−0.7/0.6	−1.3/1.5
CMSL–CM	−0.5/0.5	−0.9/1.0	−1.2/1.3

Table 2. Minimum (<0) and maximum (>0) amplitudes (in nanoteslas) of the residual field calculated at satellite altitude at dawn, dusk and noon local times for SH degrees in the range 1–12. The residual field is calculated for (OMR–OM) and (OM2B–OM). The blocks in OM2B have an electrical conductivity of 1 S m^{-1}.

Model	Dawn min/max (nT)	Dusk min/max (nT)	Noon min/max (nT)
OMR–OM	−1.2/1.9	−1.0/1.8	−2.5/1.4
OM2B–OM	−1.3/1.6	−1.1/1.0	−1.3/1.6

anomaly field for (OMSL–OM) and (CMSL–CM), respectively. As mentioned earlier, the residual contains the anomaly field associated with the mantle heterogeneity plus the mutual coupling between this heterogeneity and the coast effect. The residual field is stronger in Fig. 6(b) than in (c) and more widely spread. This results from the mutual coupling, which is stronger for the OMSL model than for the CMSL model because the OM model is more conductive than the CM model. While the effect of mantle heterogeneity is weak (Fig. 6c), it is enhanced when the mantle is conductive (Fig. 6b). In Fig. 6(b), note the slight enhancement of the anomaly amplitude in the subducting zones—for example, along Indonesia. One reason why the enhancement is not very evident is the use of the solar quiet diurnal field Sq as an inducing source field: the coast effect impacts the periods that characterize Sq (e.g. Tarits 1994). Table 1 gives the minimum and maximum amplitudes of the residual field at dawn, dusk and noon for SH degrees in the range 1–12.

Fig. 7 shows the *Z* component of the residual field calculated at noon local time for (OMR–OM) and (OM2B–OM) with SH degrees in the range 1–12. The electromagnetically induced anomaly field calculated from model OM is also included for comparison. From the figure it can be seen that the mantle heterogeneity is clearly responsible for substantial magnetic enhancements (see also Tables 1 and 2).

In Fig. 7(a), negative and positive anomalies are reinforced in the South and North Pacific next to and along the imposed ridge

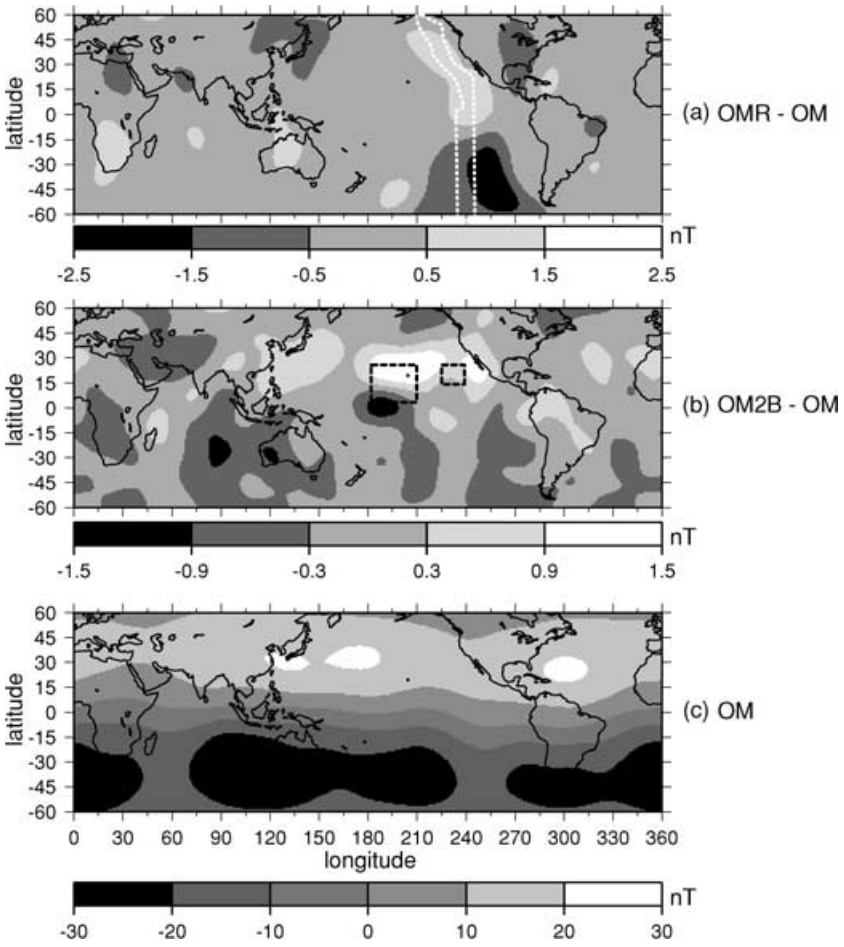

Figure 7. *Z* component of the residual field calculated at noon local time for (a) (OMR–OM) and (b) (OM2B–OM) with SH degrees in the range 1–12. The electromagnetically induced field associated with (c) model OM is included for comparison. The blocks in model OM2B have an electrical conductivity of 1 S m^{-1}. The dotted lines in (a) and (b) are a schematic representation of the heterogeneities (ridge and blocks) in the mantle.

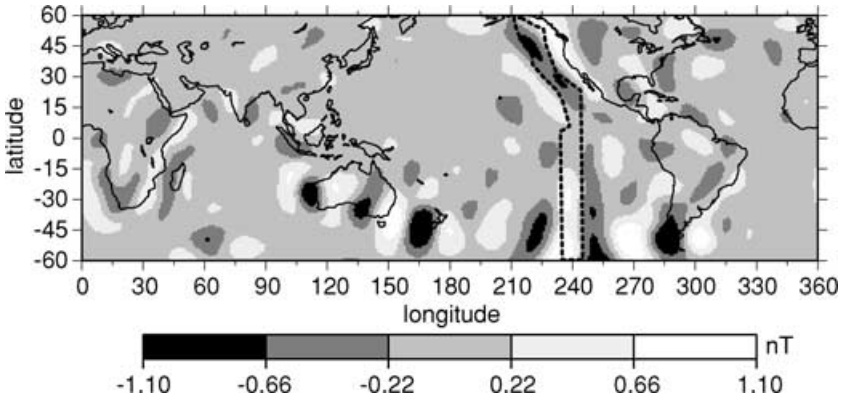

Figure 8. *Z* component of the electromagnetically induced anomaly field calculated at an altitude of 400 km at dawn local time for model OMR using a SHE with SH degrees in the range 13–27. Dawn local time is chosen as the effect of the ridge is most visible at that local time. The dotted line is a schematic representation of the ridge.

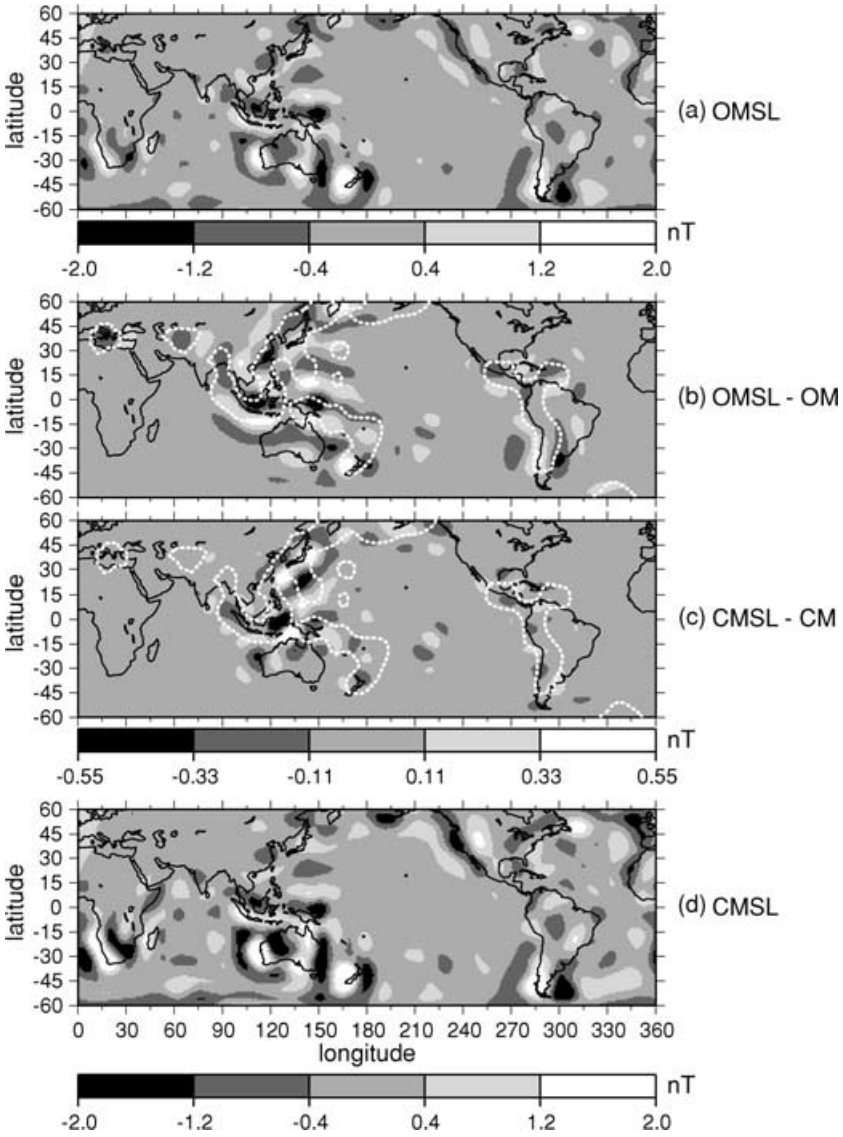

Figure 9. (a) and (d) *Z* component of the electromagnetically induced field for OMSL and CMSL, respectively. (b) and (c) *Z* component of the residual field for (OMSL–OM) and (CMSL–CM), respectively. Local time = noon. The SHE of the calculated fields contain SH degrees in the range 13–27. The slabs in OMSL have an electrical conductivity of 0.002 S m^{-1}. The second grey-scale from the bottom describes (b) and (c). The dotted white lines in (b) and (c) are a schematic representation of the subducting slabs.

structure in comparison with Figs 7(b) and 6(b). In Fig. 7(b), changes in the geometry of the magnetic anomaly distribution in the North Pacific Ocean owing to the electrically conducting blocks in the underlying mantle are clearly observed.

It can be seen (Table 2) that for wavelengths associated with SH degrees in the range 1–12, the residual field has an absolute amplitude that can reach up to 3 nT at noon local time at an altitude of 400 km. Thus, in addition to the coast effect, deep-seated electrical heterogeneities affect the long-wavelength anomaly distribution at satellite altitudes, suggesting that a long-wavelength electromagnetically induced signal arising from deep electrical conductivity contrasts is detectable at satellite altitude.

Note from both Tables 1 and 2 that the residual field amplitude depends on the local time at which the field is calculated and that it generally reaches the highest values at noon local time.

4.2.2 Residual magnetic anomaly field for SH degrees in the range 13–27

In the wavelength range associated with SH degrees between 13 and 27 (maps not shown), the electromagnetically induced anomaly fields derived from models with a heterogeneously electrically conducting mantle (OMSL, OM2B and OMR) do not, for the most part, display any outstanding magnetic signature of the electrical conductivity heterogeneities.

An exception is the electromagnetically induced anomaly field calculated from the model in which a simple representation of a ridge is used (model OMR), shown in Fig. 8. This figure represents the electromagnetic effect of a ridge but it also includes the coast effect in the SH degree range 13–27. This figure shows that the extended distribution of the electrical conductivity of a spreading centre can contribute a magnetic signal at satellite altitude. An elongated magnetic anomaly trending north–south along the ridge structure is clearly seen. The induced anomaly field reaches a maximum absolute amplitude of 2 nT at dawn or dusk local times and 3 nT at noon local time, at satellite altitude.

As mentioned earlier, Tarits & Menvielle (1983) show that for short wavelengths of the induced magnetic field (i.e. much shorter than the inducing field wavelength) and for a penetration depth exceeding the thickness of the heterogeneously electrically conducting earth layer, the mutual coupling term is negligible. To show this, we calculate residual fields for (CMSL–CM), (OMSL–OM),

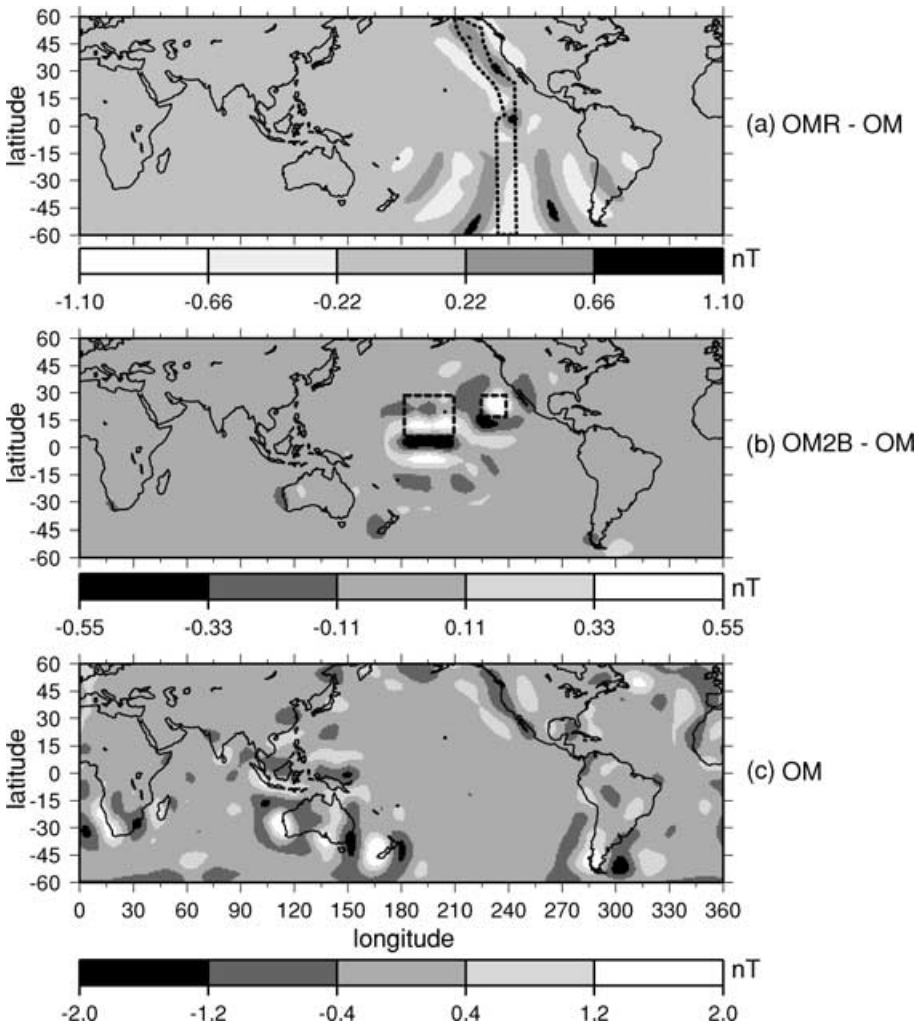

Figure 10. *Z* component of the residual field calculated at noon local time for (a) (OMR–OM) and (b) (OM2B–OM) with SH degrees in the range 13–27. The electromagnetically induced field associated with (c) model OM is included for comparison. The blocks in model OM2B have an electrical conductivity of 1 S m^{-1}. The dotted lines in (a) and (b) are a schematic representation of the heterogeneities ridge and blocks in the mantle.

Table 3. Minimum (<0) and maximum (>0) amplitudes (in nanoteslas) of the residual fields calculated at satellite altitude at dawn, dusk and noon local times for SH degrees in the range 13–27. The residual field is calculated for (OMR–OM), (OM2B–OM) and (OMSL–OM). The slabs in OMSL have an electrical conductivity of 0.002 S m^{-1} and the blocks in model OM2B have an electrical conductivity of 1 S m^{-1}.

Model	Dawn min/max (nT)	Dusk min/max (nT)	Noon min/max (nT)
OMR–OM	−0.90/1.3	−0.90/1.05	−0.59/0.81
OM2B–OM	−0.25/0.29	−0.54/0.32	−0.63/0.94
OMSL–OM	−0.34/0.22	−0.26/0.33	−0.56/0.52

(OMR–OM) and (OM2B–OM) as in the previous section. The residual fields described by SH degrees in the short-wavelength range 13–27 are shown in Figs 9 and 10.

As can be seen from Fig. 9, the mutual coupling is lower than in the case of the residual fields in the 1–12 SH degree range (Fig. 6).

Fig. 10 shows the *Z* component of the residual fields calculated at noon local time for (OMR–OM) and (OM2B–OM). The electromagnetically induced anomaly field associated with model OM is also included for comparison.

From Fig. 10 it can also be observed that the mutual coupling between the mantle heterogeneities and the coast effect is lower than in the case of the 1–12 SH degree range (see Fig. 7). Even though the amplitudes of the residual fields are weak (Table 3), Fig. 10 clearly shows that the magnetic anomaly field related to electrical heterogeneities in the mantle can be distinguished from the coast effect.

To a first approximation it may thus be possible to correct for the coast effect and extract from observed satellite magnetic data sampled at different local times, the induced anomaly field arising from electrically conducting structures in the mantle.

5 CONCLUSION

The effect of a heterogeneously conducting earth on satellite level electromagnetic anomalies was investigated using five different Earth models and spherical harmonics in two different SH degree ranges, respectively, 1–12 and 13–27.

The Earth models all have an uppermost shell with a land–ocean electrical conductivity distribution and a mantle that is either homogeneous or that contains electrical conductivity heterogeneities such as subducting slabs, a ridge, or conductive blocks.

In the 1–12 SH degree range, the electromagnetically induced field corresponds to the superposition of the magnetic response of a spherically symmetric Earth and the response arising from electrical heterogeneities in the mantle. Wavelengths associated with SH degrees in the range 1–12 overshadow any magnetic signature of electrical heterogeneities in the mantle and represent rather the average response of a spherically symmetric Earth. The electromagnetic signature associated exclusively with electrical heterogeneities in the mantle, in the 1–12 SH degree range, can be distinguished from the coast effect when a model of the induced magnetic field arising from the coast effect is subtracted from the calculated total induced magnetic field. The amplitude of the residual anomaly field is considerable and can reach up to 3 nT in absolute value, at satellite altitude and at noon local time. However, a mutual coupling between the mantle electrical heterogeneity and the coast effect is observed. While the effect of mantle heterogeneity alone is weak, we showed that it is enhanced when the mantle is conductive.

For short wavelengths associated with SH degrees in the range 13–27, the mutual coupling is weaker than in the case of SH degrees in the range 1–12. Nevertheless, the electromagnetic signature amplitude associated exclusively with electrical heterogeneities in the mantle is quite low but it is expected that an inducing source field with a stronger amplitude would produce an electromagnetically induced anomaly field with a higher amplitude.

It has also been shown that the induced magnetic anomaly field amplitude depends on the local time at which it is calculated and that it generally reaches the highest values at noon local time, irrespective of the SH degree range.

ACKNOWLEDGMENTS

The work has been carried out as part of a Community training project financed by the European Commission in the Training and Mobility of Researchers programme. The authors acknowledge the support provided by CNES (Centre National d'Etudes Spatiales) and thank Alexei Kuvshinov and an anonymous reviewer for very useful and helpful comments.

REFERENCES

Arkani-Hamed, J. & Strangway, D.W., 1987. An interpretation of magnetic signatures of subduction zones detected by MAGSAT, *Tectonophysics,* **133,** 45–55.

Counil, J.L., Cohen Y. & Achache J., 1991. The global continent–ocean magnetization contrast, *Earth planet. Sci. Lett.,* **103,** 354–364.

Didwall, E.M., 1984. The electrical conductivity of the upper mantle as estimated from satellite magnetic field data, *J. geophys. Res.,* **89,** 537–542.

Dyment, J. & Arkani-Hamed, J., 1998. Contribution of lithospheric remanent magnetization to satellite magnetic anomalies over the world's oceans, *J. geophys. Res.,* **103,** 15 423–15 441.

Egbert, G.D. & Booker, J.R., 1992. Very long period magnetotellurics at Tucson observatory: implications for mantle conductivity, *J. geophys. Res.,* **97,** 15 099–15 112.

Everett, M.E., Constable, S. & Constable C.G., 1999. Modelling 3-D induction effects in satellite data, *Expanded abstract at 2nd Symp. on 3-D Electromagnetics, Salt Lake City,* pp. 63–66.

Filloux, J.H., 1980. Magnetotelluric soundings over the North-East Pacific may reveal spatial dependence of depth and conductance of the asthenosphere, *Earth planet. Sci. Lett.,* **46,** 244–252.

Hagger, B.H. & Clayton, R.W., 1989. Constraints on the structure of mantle convection using seismic observations, flow models and the geoid, *Mantle Convection,* ed. Peltier, W.R., pp. 657–764, Gordon and Breach, New York.

Hayling, K.L., 1991. Magnetic anomalies at satellite altitude over continent–ocean boundaries, *Tectonophysics,* **192,** 129–143.

Hermance, J.F., 1982. Model simulations of possible electromagnetic effects at MAGSAT activities, *Geophys. Res. Lett.,* **9,** 373–376.

Langel, R.A., 1975. Internal and external storm-time magnetic fields from spacecraft data, abstract, *IAGA Program Abstracts for XVI General Assembly,* IUGG Pub. Office, Paris.

Langel, R.A., Sabaka, T.J., Baldwin, R.T. & Conrad, J.A., 1996. The near-earth magnetic field from magnetospheric and quiet-day ionospheric sources and how it is modeled, *Phys. Earth planet. Inter.,* **98,** 235–267.

Larsen, J.C., 1975. Low frequency (0.1–6.0 cpd) electromagnetic study of deep mantle conductivity beneath the Hawaiian Islands, *Geophys. J. R. astr. Soc.,* **43,** 17–46.

Lizarralde, D., Chave, A., Hirth, G. & Schultz, A., 1995. Northeastern Pacific mantle conductivity profile from long period magnetotelluric sounding using Hawaii-to-California submarine cable data, *J. geophys. Res.,* **100,** 17 837–17 854.

Lognonné, P., 1989. Modélisation des modes propres de vibration dans une terre anélastique et hétérogène: théorie et applications, *PhD thesis,* University Paris VII.

Menvielle, M., Rossignol, J.C. & Tarits, P., 1982. The coast effect in terms of deviated electric currents: a numerical study, *Phys. Earth planet. Inter.,* **28,** 118–128.

Mochizuki, E., 1988. Generalized spherical harmonic expansion of a solenoidal vector, *J. Geomag. Geoelectr.,* **40,** 1035–1042.

Oldenburg, D.W., Whittall, K.P. & Parker, R.L., 1984. Inversion of ocean bottom magnetotelluric data revisited, *J. geophys. Res.,* **89,** 1829–1833.

Olsen, N., 1999. Induction studies with satellite data, *Surv. Geophys.,* **20,** 309–340.

Oraevsky, V.N., Rotanova, N.M., Dimitrev, V.I., Bondar, T.N. & Abramova, D.Y., 1992a. The result of deep magnetovariational probing of the Earth according to surface data and MAGSAT satellite measurements, *Geomagn. Aeron.,* **33,** 235–239.

Oraevsky, V.N., Rotanova, N.M., Dmitriev, V.I., Semenov, V.Y., Bondar, T.N. & Abramova, D.Y., 1992b. Global magnetovariational sounding of the Earth according to MAGSAT satellite data, *Geomag. Aeron.,* **32,** 365–371.

Oraevsky, V.N., Rotanova, N.M., Bondar, T.N., Abramova, D.Y. & Semenov, V.Y., 1993a. On the radial geoelectrical structure of the mid-mantle from magnetovariational sounding using MAGSAT data, *J. Geomagn. Geoelectr.,* **45,** 1415–1423.

Oraevsky, V.N., Rotanova, N.M., Semenov, V.Y., Bondar, T.N. & Abramova, D.Y., 1993b. Magnetovariational sounding of the Earth using observatory and MAGSAT data, *Phys. Earth planet. Inter.,* **78,** 119–130.

Parkinson, W.D., 1959. Directions of rapid geomagnetic fluctuations, *Geophys. J.,* **2,** 1–14.

Parkinson, W.D., 1980. Induction by Sq, *Electromagnetic Induction in the Earth and Moon,* ed. Schmucker, U., Reidel, Dordrecht.

Phinney, R.A. & Burridge, R., 1973. Representation of the elastic–gravitational excitation of a spherical Earth model by generalized spherical harmonics, *Geophys. J. R. astr. Soc.,* **34,** 451–487.

Purucker, M.E. & Dyment J., 2000. Satellite magnetic anomalies related to seafloor spreading in the South Atlantic Ocean, *Geophys. Res. Lett.,* **27,** 2765–2768.

Schultz, A., Kurtz, R.D., Chave, A.D. & Jones, A.J., 1993. Conductivity discontinuities in the upper mantle beneath a stable craton, *Geophys. Res. Lett.,* **20,** 2941–2944.

Sclater, J.C., Jaupart, C. & Galson, D., 1980. The heat flow through oceanic and continental crust and the heat loss of the Earth, *Rev. Geophys.,* **18,** 269–311.

Shive, P.N., Frost, B.R. & Peretti A., 1988. The magnetic properties of metaperidotic rocks as a function of metamorphic grade: implications for crustal magnetic anomalies, *J. geophys. Res.,* **93,** 12 187–12 195.

Tarits, P., 1986. Conductivity and fluids in the oceanic upper mantle, *Phys. Earth planet. Inter.,* **42,** 215–226.

Tarits, P., 1994. Electromagnetic studies of global geodynamic processes, *Surv. Geophys.,* **15,** 209–238.

Tarits, P. & Menvielle, M., 1983. Etude du champ magnétique anormal d'origine intralithosphérique, *Can. J. Earth Sci.,* **20,** 537–547.

Tarits, P. & Jouanne, V., 1990. Résultats de sondages magnétotelluriques sous-marins et structure thermique de la lithosphère océanique, *Bull. Soc. Géol. Fr.,* **6,** 921–931.

Tarits, P. & Grammatika, N., 2000. Electromagnetic induction effects by Sq at MAGSAT altitude, *Geophys. Res. Lett.,* **27,** 4009–4012.

Toft, P.B. & Arkani-Hamed, J., 1992. Magnetization of the Pacific Ocean lithosphere deduced from MAGSAT data, *J. geophys. Res.,* **97,** 4387–4406.

Wannamaker, P.E., Booker, J.R., Jones, A.G., Chave, A.D., Filloux, J.H., Waff, H.S. & Law, L.K., 1989. Resistivity cross section through the Juan de Fuca subduction system and its tectonic implications, *J. geophys. Res.,* **94,** 14 127–14 144.

APPENDIX: GENERALIZED SPHERICAL HARMONIC EXPANSION (GSHE) OF MAXWELL EQUATIONS

Let $\mathbf{B}(r, \theta, \varphi)$ with components $(B_r, B_\theta, B_\varphi)$ be a vector function of position in the spherical coordinate system $(\hat{\mathbf{e}}_r, \hat{\mathbf{e}}_\theta, \hat{\mathbf{e}}_\varphi)$, r is the radius, θ the colatitude and φ the longitude. The GSH vector canonical basis is (e.g. Phinney & Burridge 1973):

$$\begin{bmatrix} \hat{\mathbf{e}}^+ \\ \hat{\mathbf{e}}^0 \\ \hat{\mathbf{e}}^- \end{bmatrix} = \begin{bmatrix} \frac{1}{\sqrt{2}}(\hat{\mathbf{e}}_\theta - i\hat{\mathbf{e}}_\varphi) \\ \hat{\mathbf{e}}_r \\ \frac{-1}{\sqrt{2}}(\hat{\mathbf{e}}_\theta + i\hat{\mathbf{e}}_\varphi) \end{bmatrix}. \tag{A1}$$

In this basis, the vector $\mathbf{B}$ has the form

$$\mathbf{B}(r, \theta, \varphi) = \sum_{-1,0,1}^{N} B^N(r, \theta, \varphi)\hat{\mathbf{e}}^N \quad (N = -1, 0, +1) \tag{A2}$$

and its GSHE is

$$\mathbf{B}(r, \theta, \varphi) = \sum_{-1,0,1}^{N} \sum_{l=0}^{\infty} \sum_{m=-l}^{l} B_l^{Nm}(r) Y_l^{Nm}(\theta, \varphi)\hat{\mathbf{e}}^N \tag{A3}$$

Here $Y_l^{Nm}(\theta, \varphi) = P_l^{Nm}(\cos\theta)\mathrm{e}^{im\varphi}$ are generalized spherical harmonics (GSHs) (Phinney & Burridge 1973), normalized so that

$$\int_0^{2\pi} \int_0^{\pi} Y_l^{Nm} \left(Y_l^{Nm}\right)^* \sin\theta \, d\theta \, d\varphi = \frac{4\pi}{2l+1} \tag{A4}$$

where $(Y_l^{Nm})^*$ is the complex conjugate of Y_l^{Nm}. Note that the B_l^{0m} are the GSH coefficients of the radial component of the vector $\mathbf{B}$. The Y_l^{0m} term is the usual scalar SH with the normalization given by eq. (A4). A comparison between GSH and regular scalar SH is given in (e.g. Mochizuki 1988).